

Atomic-scale measurement of localized dislocation phonons at Si/Ge interface

Yuehui Li^{1,2}, Bo Han^{1,2}, Ruochen Shi^{1,2}, Ruishi Qi², Xiaorui Hao², Ning Li², Bingyao Liu², Jinlong Du², Ji Chen^{3,4,5}, Peng Gao^{1,2,4,5*}

¹International Center for Quantum Materials, School of Physics, Peking University, Beijing, 100871, China

²Electron Microscopy Laboratory, School of Physics, Peking University, Beijing, 100871, China

³Institute of Condensed Matter and Material Physics, School of Physics, Peking University, Beijing, 100871, China

⁴Interdisciplinary Institute of Light-Element Quantum Materials and Research Center for Light-Element Advanced Materials, Peking University, Beijing 100871, China.

⁵Collaborative Innovation Centre of Quantum Matter, Beijing 100871, China

*Corresponding author. E-mail: p-gao@pku.edu.cn

The nanoscale lattice imperfections, such as dislocations, have a significant impact on the thermal transport properties in non-metallic materials. Understanding such effects requires the knowledge of defect phonon modes, which however is largely unexplored in experiments due to the challenge in characterization of phonons for the atomic-sized defects. Here, at the atomic scale we directly measure the localized phonon modes of dislocations at a Si/Ge interface using scanning transmission electron microscopy electron energy loss spectroscopy. We find that the dislocation induces new phonon modes localized within ~2-unit cells of the core, which experience a redshift of several milli-electron-volts compared to the dislocation-free case. The observed spectral features agree well with simulations. These localized modes are expected to reduce the phonon

transmission channels across the defect and thus the local thermal conductivity. The revealed phonon modes localized at dislocations may help us to improve the thermal properties in thermoelectric generators and thermal management systems with proper defect engineering.

The atomic-scale and nanoscale lattice imperfections such as heterointerface, interface roughness, element disorder, grain boundary and dislocation, usually have unique phonon scattering behaviors different from the bulk matrix and thus a significant impact on thermal properties¹⁻⁴ in the phonon-dominated materials and devices such as thermal management materials⁵⁻⁷ and thermoelectric devices⁸⁻¹¹. Therefore, probing the phonon modes and scattering behavior at these imperfections/interfaces is the key to understand the underlying physics of their thermal properties (e.g., thermal boundary conductance (TBC)) and subsequently gain insights into the optimization. Indeed, numerous strategies are reported to control and tune the TBC by introducing intermediate matching layer¹², ion irradiation^{13,14}, dislocations^{15,16} and so on. For example, the TBC across Al/Si interfacial region can be enhanced by up to 33% after ion irradiation due to the ion beam mixing of the native oxide and silicon¹⁴. The dislocations can reduce the TBC across the GaSb/GaAs interface by nearly a factor of two¹⁵. Those dislocations within grain boundaries of PbSb enhance the phonon scattering, resulting in a high thermoelectric performance¹⁷. The in-grain dislocation-induced lattice strain fluctuations broaden the phonon dispersion and minimize the TBC, leading to an extraordinary figure of merit of ~ 2.5 in PbTe alloys¹⁸.

However, most of these works on TBC is based on either theoretical calculations or macroscale thermal transport experiments, while little work has experimentally measured the nanoscale phonon modes and scattering behavior at imperfections, mainly because the common methods to characterize thermal conductivity usually suffer from a poor spatial resolution. Luckily, recent progress in electron energy loss spectroscopy (EELS) equipped with a monochromator in an aberration corrected scanning transmission electron microscope (STEM) has made it possible to measure localized

vibrational spectra at nanoscale and atomic-scale^{19–28} and even correlate the localized defect phonons with thermal transport properties^{29–31}.

In this work, we combine such monochromatic STEM-EELS experiments and molecular dynamics (MD) simulations with neural network force field to investigate the localized phonon modes of dislocations at a Silicon-Germanium (Si/Ge) interface. Si/Ge alloy is an excellent thermoelectric material with wide applications in thermoelectric generators converting heat flows into useable electrical energy^{32,33} and thermoelectric microrefrigerators providing large cooling power densities^{34,35}, e.g. the thermal energy of radioactive heat sources³⁶. Several methods have been proposed to engineer the thermoelectric properties of SiGe alloys, such as nanostructured SiGe alloys³⁷, SiGe/Si superlattices³⁸, defects³⁹, etc. However, the localized phonons of dislocations in such a system are still unknown and thus motivated this study.

We find that the interface dislocation strongly alters the lattice vibrational states near the dislocation core, generating the localized dislocation phonon modes confined within ~two-unit cells. The phonon energies of dislocation modes experience a redshift of several milli-electron-volts (lower than that of both Si and Ge), which is expected to reduce the transmission channels for phonons across the interface and thus the TBC. Our study unveils the localized phonon modes of individual dislocations at the Si/Ge interface, which should be useful to design better devices with desired thermal properties via dislocation engineering.

Figure 1a shows an atomically resolved high angle annular dark field (HAADF) image of a Si/Ge heterojunction interface. The lattice constant of Ge, $d_{\text{Ge}}=5.66 \text{ \AA}$, is approximately 4% larger than that of Si, $d_{\text{Si}}=5.43 \text{ \AA}$, leading to formation of misfit edge dislocations at the interface as shown in Fig. 1b. Moreover, the element distribution maps from core-loss measurement in the Supplementary Fig. 1 and the Z-contrast of Fig.1b show that the element inter-diffusion between Ge and Si occurs to form a disordered SiGe mixing layer with a thickness of about 2 nm. Figure 1c shows the phonon dispersions and phonon density of states (PDOS) of Si and Ge calculated

employing molecular dynamics based on DeePMD-kit, a package for deep learning neural network force field⁴⁰.

Figure 1d shows the acquired EEL spectra in bulk Si, bulk Ge, interfacial mixing layer at the dislocation-free region, and interfacial dislocation core using off-axis geometry⁴¹. The spectra are averaged from a spatially resolved map with the standard error shadowed. To simplify the description of experimental data, the phonons are classified into three branches, labeled as α (arrows without a tail), β (arrows with a tail) and γ . According to phonon dispersion and PDOS in Fig. 1c, α , β and γ are assigned to transverse acoustic (Si-TA) mode, longitudinal acoustic/optical (Si-LAO) mode and transverse optical (Si-TO) mode in Si side, respectively. In Ge layer, α and β are assigned to Ge-TA mode and Ge-AO (LA, LO, and TO all contribute) mode, respectively. Note that the γ phonon is pronounced only in the Si layer, while absent in the Ge layer. The α and β peaks in mixing layer are between those in bulk Si and bulk Ge. However, α and β peaks at dislocation core have lower energy than either of them, indicating new localized defect modes caused by the dislocation.

Figure 2a shows energy-filtered EELS intensity maps of window 6-14 meV, which is mainly attributed to the dislocation based on Fig. 1d. It can be clearly seen that the integrated intensity is concentrated at the dislocation core, indicating its high localization. To quantitatively validate these spectral features, the background-subtracted EEL spectra were fitted using a simple Gaussian peak fitting model. The energy distribution maps of α , β and γ phonon branches are shown in Figs. 2b-d, respectively (see supplementary Fig. 2 for the intensity distribution maps). Notably, near the dislocation core, three phonon branches all show redshift probably due to the local strain field near the dislocation core induced weakening of the bond strength⁴². In contrast, at the mixing layer away from the dislocation core (dislocation-free interfacial region), the phonon energies of α and β modes gradually transform from Si on the left to Ge on the right, which act as phonon bridges to connect significantly different energies of phonons^{31,43}. Therefore, the interfacial dislocation has very different

localized phonon modes than the dislocation-free case, implying its important influence on the thermal transport properties.

Figure 2e shows the extracted line profiles of α , β and γ phonon energy through the mixing layer (black) and interface dislocation (red) along the X direction (perpendicular to the interface) denoted by the solid rectangles in Fig. 2a, where all of the dislocation-induced localized modes, α_{disl} , β_{disl} , and γ_{disl} modes show redshift at the dislocation core (0 nm). Specifically, the energy of α_{disl} mode is ~ 1.2 meV lower than that of bulk Ge-TA mode, the energy of β_{disl} mode is ~ 3.1 meV lower than that of bulk Ge-AO mode, and the energy of γ_{disl} mode is ~ 2.3 meV lower than that of the regular interface mode. Figure 2f and Supplementary Fig. 3 show the phonon energy changes of α , β and γ modes through the dislocation core along the Y direction (parallel to the interface) denoted by the dotted rectangle in Fig. 2a. The corresponding Gaussian fitted line profiles have a full width of half maximum of ~ 1.18 nm for α_{disl} , ~ 1.17 nm for β_{disl} and ~ 1.17 nm for γ_{disl} respectively, indicating highly localized nature of the dislocation phonon modes. In contrast, the phonon intensity distribution is much less affected by the presence of dislocation as shown in the supplementary Fig. 2.

To further understand the effects of dislocation on localized phonons, Figure 3a shows the calculated PDOS of Si/Ge system without (black) and with (red) interface dislocations by molecular dynamics, respectively. The system is divided into 6 regions, of which the third and fourth layers locate at the interface, the second and fifth layers are close to the interface, the first and sixth layers are far from the interface. Away from the interface, regions 1, 2, 5, and 6 are less influenced thus the PDOS basically overlap for both cases. In the third region, the dislocation-free interface mode at 47.5 meV originates from the vibration of Si-Ge bonds and disappears in the Ge layer, which is consistent with the experiment that γ mode only exists in Si layer. The strain field at the dislocation weakens the strength of Si-Ge bonds (mainly from vibrations of Si atoms), thus making the vibrational energy of Si-Ge bonds redshift, i.e., the γ_{disl} mode is ~ 2 meV lower than the dislocation-free interface mode. In contrast, the redshift of α_{disl}

mode and β_{disl} mode is mainly related to the low-frequency vibrations of Ge atoms induced by dislocations, as shown in the fourth layer. The α_{disl} mode is ~ 2.2 meV lower than the Ge-TA mode, and the β_{disl} mode is ~ 1.4 meV lower than the Ge-AO mode. In order to better reproduce the experimental conditions, a mixing layer is also modeled, as shown in Fig. 3b. With the mixing layer, the α_{dis} mode is ~ 1.4 meV lower than the Ge-TA mode, the β_{disl} mode is ~ 4.4 meV lower than the Ge-AO mode, and the γ_{disl} mode is ~ 2.1 meV lower than the dislocation-free case, which is more consistent with the experimental results, as shown in Fig. 3c.

Now we briefly discuss how the thermal transport properties are influenced by the dislocation and interface disorder layer. The number of heat channels is closely related to the PDOS overlap according to the diffuse mismatch model, and the higher (lower) the PDOS overlap, the more (less) phonon scattering channels^{44,45}. The energy of localized mode at the dislocation core is substantially lower than that of the bulk phonon on both sides, which are expected to reduce the number of phonon channels that can pass through the interface through inelastic scattering by reducing the PDOS overlap. Meanwhile, the dislocations also reduce the group velocity of phonons accompanied by the redshift of phonon energies⁴². Both effects lead to the reduction of the TBC¹⁶. The reduction of thermal conductivity is beneficial for the enhancement of thermoelectric performance. For example, previous study reported that the scattering of a wide spectrum of phonons by dislocations, grain boundaries and other imperfections in SiGe alloys leads to a significantly low thermal conductivity ~ 0.93 W/(m·K), and thus enhance the thermoelectric figure-of-merit ~ 1.84 at 1073 K⁴⁶. In fact, besides SiGe alloys, dislocations were also introduced into many other thermoelectric materials to obtain high performance^{47,48}. In addition, it should be noted that the mixing layer also influence the phonon transport. Previous study reported the presence of the interface phonons at the Si/Ge interface²⁹ contributes to $\sim 5\%$ of the total TBC via inelastic processes at 300 K. With the mixing layer, our work indicates that the low-frequency α and β phonon modes act as bridges to connect phonons with significantly different

energies on two sides^{31,43}, as shown in Fig. 2e. Therefore, phonons can pass across the interface through the new scattering channels, leading to enhancement of the TBC. Moreover, the improvement originating from low-frequency phonons may contribute more due to Bose-Einstein distribution. More details about the effects of disordered mixing layer are provided in Supplementary Information. In our practical case with both of dislocation and interdiffusion at the interface, the effects on thermal transport are even more complicated due to not only their competitions but also their interactions. For example, the phonon energy near the dislocation is also lower than that away from the dislocation. This is partly because the dislocation lowers the activation energy for diffusion⁴⁹⁻⁵¹, resulting in the higher Ge content near the dislocation core (as shown in Supplementary Figs. 1a-c) which supposed to have lower phonon energies. Therefore, the dislocation and interdiffusion at the interface influence the thermal transport in a very complicated manner.

In summary, we directly measure the localized phonon modes of dislocations at the Si/Ge interface using atomically resolved STEM-EELS and MD simulations. We find that the dislocation modes caused by the edge dislocations at the interface are highly localized within ~two-unit cells near the dislocation core. Such dislocation modes experience redshift of several milli-electron-volts, lower than that of both Si and Ge, which reduce the overlap of PDOS and the number of phonon scattering channels, leading to reduction of the TBC. The experimental measurement of the local phonon modes of individual dislocations at Si/Ge interface, provides useful information for the engineering of thermal properties via defect engineering.

Methods

TEM sample preparation. The cross-sectional TEM specimen was prepared by mechanical polishing followed by an argon ion milling carried out using the Precision Ion Polishing System (Model 691, Gatan Inc.). The specimen was baked at 160 °C for 16 hours to further remove the surface amorphous layer before EELS experiments.

Experimental setup. The vibrational spectra were acquired at a Nion U-HERMES200 electron microscope equipped with both the monochromator and the aberration corrector operated at 60 kV. The convergence semi-angle and the collection semi-angle were both 25 mrad. The electron beam was moved off optical axis with ~ 80 mrad for off-axis experiments to greatly reduce the contribution of the dipole scattering⁴¹. The energy dispersion channel was set as 0.5 meV with 2048 channels in total.

MD simulation. The MD simulations were performed using the Large-scale Atomic/Molecular Massively Parallel Simulator (LAMMPS) package⁵² integrated with the DeePMD-kit, a deep learning package for many-body potential energy representation⁴⁰. First, we built a neural network force field model for Si-Ge system. The training datasets were calculated using density functional theory by Quantum ESPRESSO⁵³. The ultra-soft pseudopotential (USPP) and the Perdew-Burke-Enzerhof (PBE) exchange-correlation functional were used. We generated a series of training datasets for pure Si, pure Ge, 25%Si-75%Ge crystalline alloys, 50%Si-50%Ge crystalline alloys and 75%Si-25%Ge crystalline alloys to obtain a robust deep potential. Then we performed MD simulations with this well-trained deep potential. The simulation system generally contains $4 \times 4 \times 16$ conventional cells on both Si and Ge sides. Periodic boundary conditions are applied in all directions. To create the random atomic mixing layer, we select the 2-unit-cell-long Ge layer near the interface and randomly replace several Ge atoms as Si atoms. A time step of 1 fs was used in all simulations, which is short enough to resolve all phonon modes. Our simulations were carried out in three steps. First, we performed simulations at 300 K and zero pressure for 20 ps using the NPT ensemble with Nosé/Hoover thermostat barostat. Then the simulations were extended for another 20 ps using the NVE ensemble. The phonon density of states (PDOS) were calculated using the next 5 ps NVE simulations, which is long enough for our systems containing many atoms (see Supplementary Fig. 4). After extracting the atomic velocities along the trajectory, PDOS is obtained by the fast

Fourier transformation of velocity autocorrelation function (VACF). The PDOS projected on atom j can be calculated:

$$g_j(\omega) = \int e^{i\omega t} \frac{\langle v_j(t)v_j(0) \rangle}{\langle v(0)v(0) \rangle} dt$$

where ω is the phonon frequency, v_j is the velocity of atom j , the $\langle \dots \rangle$ brackets indicate averaging over different starting step along the trajectory. The entire simulation domain was divided into many cells, and the phonon density of states contributed by the atoms of each cell were calculated.

Acknowledgements

This work was supported by the National Key R&D Program of China (2021YFA140050) and the National Natural Science Foundation of China (52125307, 11974023, 52021006). We acknowledge the High-performance Computing Platform of Peking University for providing computational resources for the MD simulations.

Author contributions

P.G. conceived and supervised the project. Y. H. L., B. H., R. C. S. and N. L. performed the research assisted by J. L. D. and J. C.; R. S. Q. and R. C. S. contributed new reagents/analytic tools; X. R. H. and B. Y. L. fabricated the TEM sample. Y. H. L. and B. H. wrote the manuscript under the direction of P.G. with contributions from all other co-authors.

Competing interests

The authors declare no competing interests.

Figures and captions

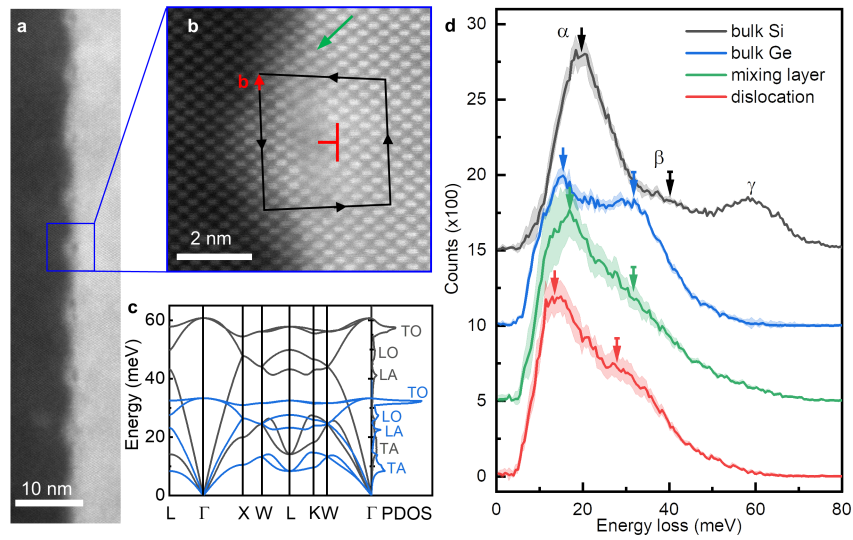


Fig. 1 | HAADF image and EEL spectra acquired at different locations. a, A HAADF image of a Si/Ge interface. **b,** An enlarged view showing the atomic structure of an interface dislocation. The Burgers vector **b** is denoted by the red arrow. The green arrow denotes the disordered mixing layer at the dislocation-free interface region based on the Z-contrast. **c,** Calculated phonon dispersions and PDOSs of Si (black) and Ge (blue). **d,** EEL spectra with standard error (shadowed region) acquired at different locations. The arrows without (with) tail denote α (β) modes.

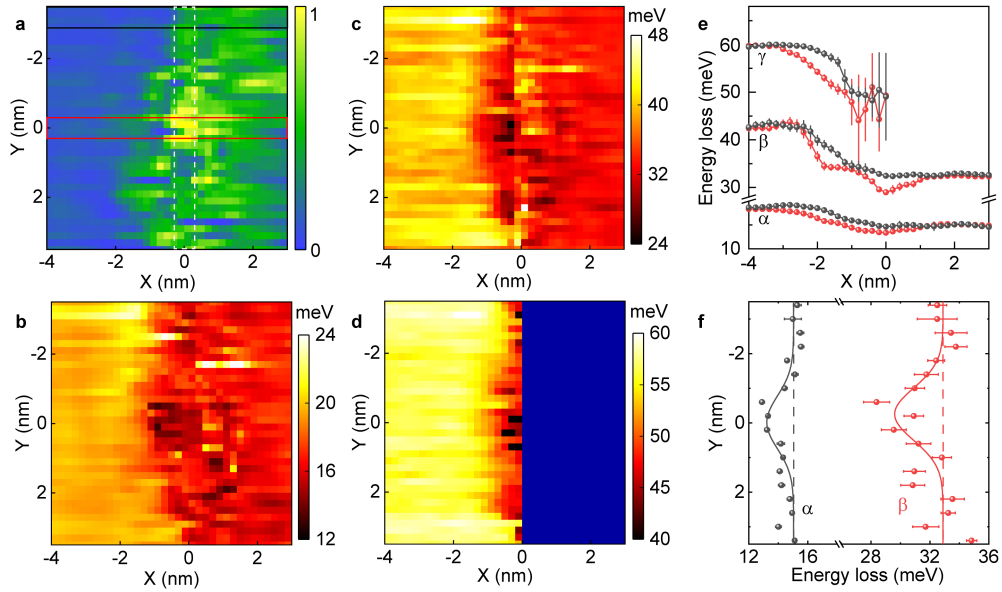


Fig. 2 | The intensity and energy distribution maps of phonons. **a**, The energy-filtered EELS intensity map of 6-14 meV window corresponding to one branch of the dislocation phonon modes. **b-d**, The energy distribution maps of α , β and γ phonon branches. The phonon energy is extracted by a simple Gaussian peak fitting model. All of them showing the lower energy at the dislocation. **e**, The line profiles of α , β and γ phonon energy through the mixing layer (black) and interface dislocation (red) along the X direction denoted by solid rectangles in **a**. **f**, The data points of the phonon energy of α , and β modes through the dislocation core along the Y direction denoted by dotted rectangle in **a**. The solid lines are the fitted Gaussian distributions.

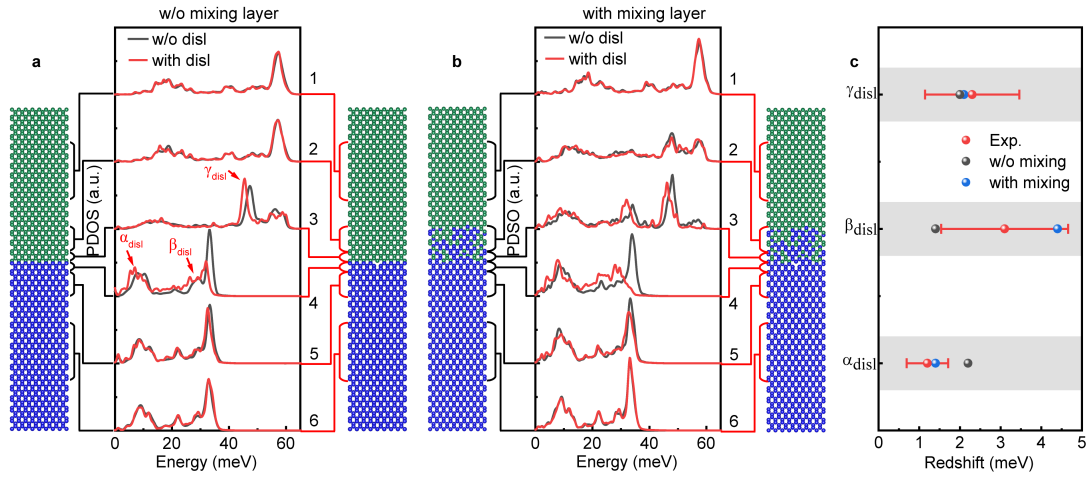


Fig. 3 | Molecular dynamics simulations of different Si/Ge systems. a, Schematic diagrams and calculated PDOS of Si/Ge systems without a mixing layer. Each layer is the PDOS of the atoms at the brace. The dislocation modes (red arrows) experience a redshift compared to dislocation-free case (black). **b,** Schematic diagrams and calculated PDOS of Si/Ge systems with a mixing layer. Redshift also occurs. **c,** The energy redshift of α_{disl} , β_{disl} and γ_{disl} branches obtained in experiments (red), simulations without a mixing layer (black) and simulations with a mixing layer (blue), respectively.

References

1. Qian, X., Zhou, J. & Chen, G. Phonon-engineered extreme thermal conductivity materials. *Nat. Mater.* **20**, 1188–1202 (2021).
2. Simoncelli, M., Marzari, N. & Mauri, F. Unified theory of thermal transport in crystals and glasses. *Nat. Phys.* **15**, 809–813 (2019).
3. Hopkins, P. E. Thermal transport across solid interfaces with nanoscale imperfections: effects of roughness, disorder, dislocations, and bonding on thermal boundary conductance. *ISRN Mech. Eng.* **2013**, e682586 (2013).
4. Merabia, S. & Termentzidis, K. Thermal boundary conductance across rough interfaces probed by molecular dynamics. *Phys. Rev. B* **89**, 054309 (2014).
5. Luckyanova, M. N. *et al.* Coherent Phonon Heat Conduction in Superlattices. *Science* **338**, 936–939 (2012).
6. Ravichandran, J. *et al.* Crossover from incoherent to coherent phonon scattering in epitaxial oxide superlattices. *Nat. Mater.* **13**, 168–172 (2014).
7. Luckyanova, M. N. *et al.* Phonon localization in heat conduction. *Sci. Adv.* **4**, eaat9460 (2018).
8. Poudel, B. *et al.* High-Thermoelectric Performance of Nanostructured Bismuth Antimony Telluride Bulk Alloys. *Science* **320**, 634–638 (2008).
9. He, R., Schierning, G. & Nielsch, K. Thermoelectric devices: a review of devices, architectures, and contact optimization. *Adv. Mater. Technol.* **3**, 1700256 (2018).
10. Chen, Z., Zhang, X. & Pei, Y. Manipulation of Phonon Transport in Thermoelectrics. *Adv. Mater.* **30**, 1705617 (2018).
11. Zhang, J. *et al.* Direct observation of one-dimensional disordered diffusion channel in a chain-like thermoelectric with ultralow thermal conductivity. *Nat Commun* **12**, 6709 (2021).
12. Polanco, C. A. *et al.* Design rules for interfacial thermal conductance: Building better bridges. *Phys. Rev. B* **95**, 195303 (2017).
13. Tao, Y. *et al.* The enhancement of heat conduction across the metal/graphite

- interface treated with a focused ion beam. *Nanoscale* **12**, 14838–14846 (2020).
14. Gorham, C. S. *et al.* Ion irradiation of the native oxide/silicon surface increases the thermal boundary conductance across aluminum/silicon interfaces. *Phys. Rev. B* **90**, 024301 (2014).
 15. Hopkins, P. E. *et al.* Effect of dislocation density on thermal boundary conductance across GaSb/GaAs interfaces. *Appl. Phys. Lett.* **98**, 161913 (2011).
 16. Sun, J., Li, Y., Karaaslan, Y., Sevik, C. & Chen, Y. Misfit dislocation structure and thermal boundary conductance of GaN/AlN interfaces. *J. Appl. Phys.* **130**, 035301 (2021).
 17. Chen, Z. *et al.* Vacancy-induced dislocations within grains for high-performance PbSe thermoelectrics. *Nat Commun* **8**, 13828 (2017).
 18. Wu, Y. *et al.* Thermoelectric enhancements in PbTe alloys due to dislocation-induced strains and converged bands. *Adv. Sci.* **7**, 1902628 (2020).
 19. Krivanek, O. L. *et al.* Vibrational spectroscopy in the electron microscope. *Nature* **514**, 209–212 (2014).
 20. Lagos, M. J., Trügler, A., Hohenester, U. & Batson, P. E. Mapping vibrational surface and bulk modes in a single nanocube. *Nature* **543**, 529–532 (2017).
 21. Hage, F. S., Kepaptsoglou, D. M., Ramasse, Q. M. & Allen, L. J. Phonon spectroscopy at atomic resolution. *Phys. Rev. Lett.* **122**, 016103 (2019).
 22. Venkatraman, K., Levin, B. D. A., March, K., Rez, P. & Crozier, P. A. Vibrational spectroscopy at atomic resolution with electron impact scattering. *Nat. Phys.* **15**, 1237–1241 (2019).
 23. Huang, S. *et al.* Recent progress of vibrational electron energy-loss spectroscopy in scanning transmission electron microscope. *Chin. J. Vac. Sci. Technol.* **41**, 213–224 (2021).
 24. Hage, F. S., Radtke, G., Kepaptsoglou, D. M., Lazzeri, M. & Ramasse, Q. M. Single-atom vibrational spectroscopy in the scanning transmission electron microscope. *Science* **367**, 1124–1127 (2020).

25. Tian, X. *et al.* Capturing 3D atomic defects and phonon localization at the 2D heterostructure interface. *Sci. Adv.* **7**, eabi6699.
26. Yan, X. *et al.* Single-defect phonons imaged by electron microscopy. *Nature* **589**, 65–69 (2021).
27. Qi, R. *et al.* Measuring phonon dispersion at an interface. *Nature* **599**, 399–403 (2021).
28. Pan, X. *et al.* *Nanoscale Imaging of Phonon Dynamics by Electron Microscopy*. Preprint at <https://www.researchsquare.com/article/rs-540715/v1> (2021).
29. Cheng, Z. *et al.* Experimental observation of localized interfacial phonon modes. *Nat Commun* **12**, 6901 (2021).
30. Hoglund, E. R. *et al.* Emergent interface vibrational structure of oxide superlattices. *Nature* **601**, 556–561 (2022).
31. Li, Y.-H. *et al.* Atomic-scale probing of heterointerface phonon bridges in nitride semiconductor. *PNAS* **119**, e2117027119 (2022).
32. Basu, R. & Singh, A. High temperature Si–Ge alloy towards thermoelectric applications: A comprehensive review. *Mater. Today Phys.* **21**, 100468 (2021).
33. Schierning, G. Silicon nanostructures for thermoelectric devices: A review of the current state of the art. *Phys. Status Solidi A* **211**, 1235–1249 (2014).
34. Su, Y., Lu, J., Villaroman, D., Li, D. & Huang, B. Free-standing planar thermoelectric microrefrigerators based on nano-grained SiGe thin films for on-chip refrigeration. *Nano Energy* **48**, 202–210 (2018).
35. Vashaee, D. *et al.* Modeling and optimization of single-element bulk SiGe thin-film coolers. *Microscale Thermophys. Eng.* **9**, 99–118 (2005).
36. Wood, C. Materials for thermoelectric energy conversion. *Rep. Prog. Phys.* **51**, 459–539 (1988).
37. Hochbaum, A. I. *et al.* Enhanced thermoelectric performance of rough silicon nanowires. *Nature* **451**, 163–167 (2008).
38. Lee, S.-M., Cahill, D. G. & Venkatasubramanian, R. Thermal conductivity of Si–

- Ge superlattices. *Appl. Phys. Lett.* **70**, 2957–2959 (1997).
39. Bathula, S. *et al.* The role of nanoscale defect features in enhancing the thermoelectric performance of p-type nanostructured SiGe alloys. *Nanoscale* **7**, 12474–12483 (2015).
 40. Wang, H., Zhang, L., Han, J. & E, W. DeePMD-kit: A deep learning package for many-body potential energy representation and molecular dynamics. *Comput. Phys. Commun.* **228**, 178–184 (2018).
 41. Dwyer, C. *et al.* Electron-beam mapping of vibrational modes with nanometer spatial resolution. *Phys. Rev. Lett.* **117**, 256101 (2016).
 42. Li, M. *et al.* Nonperturbative quantum nature of the dislocation–phonon interaction. *Nano Lett.* **17**, 1587–1594 (2017).
 43. Tian, Z., Esfarjani, K. & Chen, G. Enhancing phonon transmission across a Si/Ge interface by atomic roughness: First-principles study with the Green’s function method. *Phys. Rev. B* **86**, 235304 (2012).
 44. Swartz, E. T. & Pohl, R. O. Thermal boundary resistance. *Rev. Mod. Phys.* **61**, 605–668 (1989).
 45. Zhang, P. *et al.* A theoretical review on interfacial thermal transport at the nanoscale. *Small* **14**, 1702769 (2018).
 46. Basu, R. *et al.* Improved thermoelectric performance of hot pressed nanostructured n-type SiGe bulk alloys. *J. Mater. Chem. A* **2**, 6922–6930 (2014).
 47. Shi, X.-L., Zou, J. & Chen, Z.-G. Advanced thermoelectric design: from materials and structures to devices. *Chem. Rev.* **120**, 7399–7515 (2020).
 48. Mao, J. *et al.* Advances in thermoelectrics. *Advances in Physics* **67**, 69–147 (2018).
 49. Huang, J., Meyer, M. & Pontikis, V. Is pipe diffusion in metals vacancy controlled? A molecular dynamics study of an edge dislocation in copper. *Phys. Rev. Lett.* **63**, 628–631 (1989).
 50. Fang, Q. F. & Wang, R. Atomistic simulation of the atomic structure and diffusion within the core region of an edge dislocation in aluminum. *Phys. Rev. B* **62**, 9317–

9324 (2000).

51. Legros, M., Dehm, G., Arzt, E. & Balk, T. J. Observation of giant diffusivity along dislocation cores. *Science* **319**, 1646–1649 (2008).
52. Plimpton, S. Fast Parallel Algorithms for Short-Range Molecular Dynamics. *J. Comput. Phys.* **117**, 1–19 (1995).
53. Giannozzi, P. *et al.* QUANTUM ESPRESSO: a modular and open-source software project for quantum simulations of materials. *J. Phys.: Condens. Matter* **21**, 395502 (2009).

Supplementary Information: Atomic-scale measurement of localized dislocation phonons at Si/Ge interface

Yuehui Li^{1,2}, Bo Han^{1,2}, Ruochen Shi^{1,2}, Ruishi Qi², Xiaorui Hao², Ning Li², Bingyao Liu², Jinlong Du², Ji Chen^{3,4,5}, Peng Gao^{1,2,4,5*}

¹International Center for Quantum Materials, School of Physics, Peking University, Beijing 100871, China

²Electron Microscopy Laboratory, School of Physics, Peking University, Beijing 100871, China

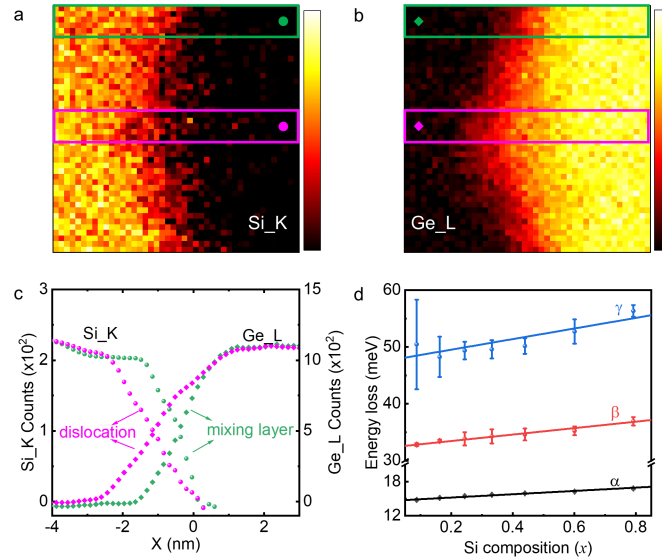
³Institute of Condensed Matter and Material Physics, School of Physics, Peking University, Beijing 100871, China

⁴Interdisciplinary Institute of Light-Element Quantum Materials and Research Center for Light-Element Advanced Materials, Peking University, Beijing 100871, China

⁵Collaborative Innovation Centre of Quantum Matter, Beijing 100871, China

*Corresponding author. E-mail: p-gao@pku.edu.cn

The disordered mixing layer at the interface and the effect on phonon modes and thermal property

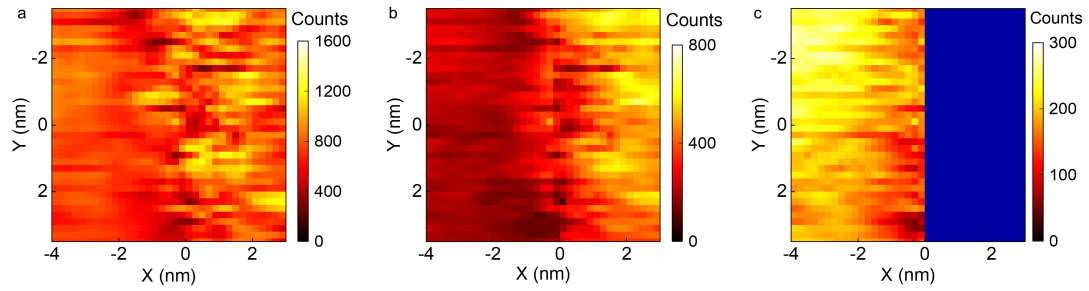


Supplementary Figure 1. The element distribution at the interface. **a**, The intensity mapping of Si_K edge extracted from the core loss EELS. **b**, The intensity mapping of Ge_L edge. **c**, The intensity line profiles of the green region (disordered mixing layer with dislocation-free) and pink region (dislocation core) in **a** and **b**. **d**, The phonon energy of α , β and γ modes as a function of the Si composition (x), calculated from intensity ratio of Si_K/(Si_K+Ge_L), in the disordered mixing layer.

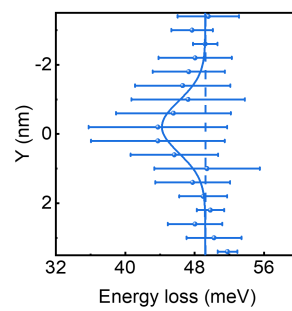
The element distribution maps extracted from core loss EELS edges (Si_K edge and Ge_L edge) are shown in Fig. S1a and S1b. The dislocation promotes the diffusion of Ge into the Si layer due to the dislocation reduced activation energy for diffusion¹⁻³, leading to a larger diffusion depth. Figure S1c shows the line profile of Si composition and Ge composition across the mixing layer (green) and interface dislocation (pink) along X direction denoted by rectangles in Fig. S1a and S1b, respectively. Approaching to the interface (0 nm) in the Si side, the Si composition becomes lower and the Ge composition becomes higher. Correspondingly, the phonon energies of α , β and γ modes gradually decrease. Figure S1d shows the energy of α , β and γ modes as a function of

the Si composition (x), intensity ratio $\text{Si_K}/(\text{Si_K}+\text{Ge_L})$, in the mixing layer. The energies of α , β and γ modes are approximately linearly related to the Si composition, with slopes of 2.91 ± 0.12 meV, 5.68 ± 0.26 meV and 9.33 ± 1.44 meV, respectively. γ mode corresponds to Si-Si and Si-Ge bonding optical vibrations with a slope lying within consistent values in literatures^{4,5}. The different effects of Si composition on Si-Si bonds, Si-Ge bonds and Ge-Ge bonds lead to different slopes of α , β and γ modes as a function of Si composition. There are two competitive effects in the disordered mixing layer. One is that as Si composition increases, the bond length decreases, which leads to an upshift of vibrational energy. The other is that the disorder-induced shorter order range leads to vibrational energy downshifts with respect to an ideal lattice⁶. That is to say, as Si composition increases, the disorder-induced upshift of vibrational frequency of Si-Si bond and the downshift of vibrational frequency of Ge-Ge bond both exist. The overall effect is that as Si composition increases, the vibrational energy of Si-Si bond strongly increases, the vibrational energy of Si-Ge bond first increases and then decreases, and the vibrational energy of Ge-Ge bond slightly decreases^{6,7}. The γ mode is above 45 meV, including the contributions of Si-Si bonds and Si-Ge bonds but not Ge-Ge bonds, so its slope is the largest. The α mode is below 18 meV, containing mainly the contribution of Ge-Ge bonds, so its slope is minimal.

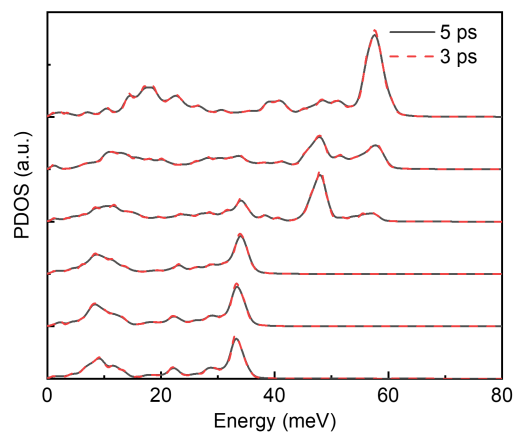
At the interface, the α mode connects the Si-TA mode and Ge-TA mode, the β mode connects the Si-LAO mode and Ge-AO mode. Therefore, the α mode and β mode gradually convert Si phonons to Ge phonons through the mixing layer, which facilitates the phonon transport through the interface and is beneficial to increase TBC⁸. On the other hand, the disorder-induced phonon backscattering reduces phonon transmittance and TBC was also reported^{8,9}. Therefore, whether the disordered mixing layer enhances or reduces TBC depends the competition of these two effects⁹.



Supplementary Figure 2. The intensity distribution maps of α (a), β (b) and γ (c) phonon branches extracted by a simple Gaussian peak fitting model.



Supplementary Figure 3. The line profile of γ mode through the dislocation core along the Y direction denoted by dotted rectangle in Fig. 2a. The solid line is the fitted Gaussian distribution.



Supplementary Figure 4. Calculated phonon density of states projected onto different layers of Si/Ge system with a mixing layer using 5 ps (black) and 3 ps (red) NVE simulations, respectively. It is clearly seen that the calculation has converged for 5 ps.

References

1. Huang, J., Meyer, M. & Pontikis, V. Is pipe diffusion in metals vacancy controlled? A molecular dynamics study of an edge dislocation in copper. *Phys. Rev. Lett.* **63**, 628–631 (1989).
2. Fang, Q. F. & Wang, R. Atomistic simulation of the atomic structure and diffusion within the core region of an edge dislocation in aluminum. *Phys. Rev. B* **62**, 9317–9324 (2000).
3. Legros, M., Dehm, G., Arzt, E. & Balk, T. J. Observation of giant diffusivity along dislocation cores. *Science* **319**, 1646–1649 (2008).
4. Alonso, M. I. & Winer, K. Raman spectra of c-Si_{1-x}Ge_x alloys. *Phys. Rev. B* **39**, 10056–10062 (1989).
5. Nakashima, S., Mitani, T., Ninomiya, M. & Matsumoto, K. Raman investigation of strain in Si/SiGe heterostructures: Precise determination of the strain-shift coefficient of Si bands. *Journal of Applied Physics* **99**, 053512 (2006).
6. de Matteis, D. *et al.* Probing Lattice Dynamics and Electronic Resonances in Hexagonal Ge and Si_xGe_{1-x} Alloys in Nanowires by Raman Spectroscopy. *ACS Nano* **14**, 6845–6856 (2020).
7. Pezzoli, F. *et al.* Raman spectroscopy determination of composition and strain in Si_{1-x}Ge_x/Si heterostructures. *Materials Science in Semiconductor Processing* **11**, 279–284 (2008).
8. Tian, Z., Esfarjani, K. & Chen, G. Enhancing phonon transmission across a Si/Ge interface by atomic roughness: First-principles study with the Green's function method. *Phys. Rev. B* **86**, 235304 (2012).
9. English, T. S. *et al.* Enhancing and tuning phonon transport at vibrationally mismatched solid-solid interfaces. *Phys. Rev. B* **85**, 035438 (2012).